第 34 卷第 4 期
2015 年 8 月

红 外 与 毫 米 波 学 报
J. Infrared Millim. Waves

Vol. 34, No. 4
August, 2015

文章编号: 1001 - 9014(2015)04 - 0420 - 07

DOI:10.11972/j.issn.1001 - 9014.2015.04.007

Compensating the effects of DC bias lines on terahertz photomixer antennas using resistively loaded lines

Adem Yilmaz, Mehmet Unlu *

(Electrical and Electr onics Engineering Department, Yildirim Beyazit University, Ankara, Turkey
Cankiri Caddesi, Cicek Sokak, No: 3, Ulus, Ankara, 06030, Turkey)

Abstract: This paper proposed a method, namely resistively loaded lines (RLL), to compensate the effects of the DC bias lines after investigating its effects on several types of antennas for terahertz photomixers. The RLL is formed by placing lumped resistances periodically on the DC bias line in order to cease the leakage current virtually, which cause a significant amount of distortion on the antenna performance. The simulation results of the dipole, folded dipole, log-periodic, and spiral antennas show that RLL almost removes the effects of the bias lines and improves the antenna radiation resistance and radiation pattern notably compared with that of the commonly used bias line types, such as coplanar stripline and photonic bandgap type bias lines.

Key words: terahertz, photomixer, antenna, DC bias line, millimeterwave
PACS: 84.40.Ba

Introduction

Terahertz technology has recently attracted considerable attention due to its potential applications on a variety of fields, examples of which are medical imaging, security, wireless communication, and material spectroscopy[1-8]. Although a great deal of effort has been spent on developing several different components for terahertz systems, the main concentration is focused on the terahertz sources and detectors[9-14], the development of which is still the most important challenge in this field. Photomixing is one of the most commonly used techniques for continuous-wave terahertz generation or detection[15-18], where two laser beams that have close frequencies excite an active semiconductor area, and the excited signal is fed into an integrated antenna. A DC voltage is needed for the operation of the photomixer, which is typically supplied using DC bias lines that are connected to the antenna terminals. The effects of these DC bias lines are investigated in detail in[39]; however, they are still mostly neglected although they have a significant effect on the radiation performance of the photomixer antenna as the dimensions of the bias line are generally much larger compared with the dimensions of the antenna itself[19, 36, 40].

One of the most popular, and easy to design, bias line type is coplanar stripline (CPS)[20]. They are basically composed of two thin metal lines, which actually behave as a high impedance transmission line between the DC supply and photomixer antenna. The dimensions of CPS are most of the time comparatively larger than the antenna; in addition to that, they are directly connected to the antenna itself, which results in a considerable amount of current leakage to the CPS, causing a significant distortion on the radiation pattern and input impedance, and a considerable loss of generated or detected power.

A better alternative for bias lines is using photonic bandgap type structures[21-22]. Photonic bandgap structures (PBG) are designed as low-pass/high-pass filters that are formed using high and low impedance CPS sections. Although the PBG bias lines are also connected directly to the photomixer antenna just as the CPS bias lines, the current leakage from the antenna can be reduced to a certain extent by a proper design; however, they still cause an important malformation on the current distribution, and hence, the radiation pattern of the antenna is distorted drastically. Moreover, the radiated power decreases due to the leakage current running on the long bias lines. As a result, these two types of bias lines affect the antenna radiation pattern and input impedance notably, they decrease the antenna efficiency; hence, a better solution is needed.

In this paper, a new type of bias line, namely resistively loaded line (RLL), was proposed for the biasing of the photomixer antennas, where the conventional CPS bias line is delimited by a set of periodically placed lumped resistances. The lumped resistances were formed using a resistive thin film that has a high and adjustable resistivity, such as silicon chromium (SiCr) or tantalum nitride (TaN), which makes it possible to adjust the resistance level specifically for each design. Different types of photomixer antennas with the CPS, PBG, and RLL bias lines have been designed in order to compare the effects of all three types of bias lines. The simulation results show that when RLL bias line is used, the photomixer antenna performance is recovered and becomes almost the same as that of the antenna without any bias lines. Moreover, using the RLL bias line improves the radiation resistance and radiation pattern of the antenna compared with the case where the CPS and PBG bias lines are used.

1 Bias line types

Figure 1 shows the layout of a generic photomixer antenna and a photograph of an example photomixer antenna[36], both of which basically consists of an antenna, bias lines, and probe pads. Different types of bias lines were employed in the literature in order to carry the required DC voltage to the antenna[18-21, 22, 23]. However, in all of these solutions, it was observed that the dimensions of the bias lines are much larger compared with the dimensions of the antenna (Fig. 1(b)), which is expected to cause a considerable distortion on the antenna performance.

Different types of bias lines are first analyzed as two-port net-

Received date: 2014 - 08 - 15, **revised date**: 2015 - 04 - 16 收稿日期:2014 - 08 - 15, 修回日期:2015 - 04 - 16
Foundation items: Supported by TUBITAK(114E089) and Yildirim Beyazit University (BAP-585)
* **Corresponding author**: E-mail: munlu@ybu.edu.tr

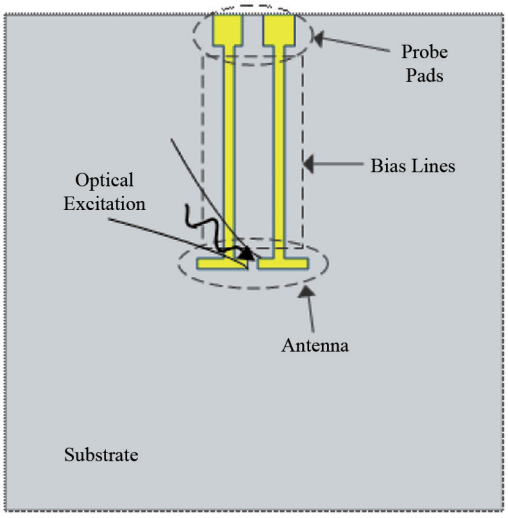

(a)

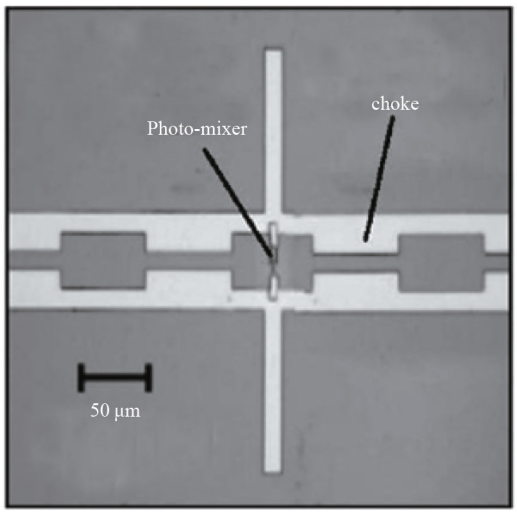

(b)

Figure 1　(a) The layout of a generic photomixer antenna (b) The photograph of an example photomixer antenna[36]

works in order to investigate the amount of leakage on the bias lines, and hence, to see how significantly the antenna performance would be affected. The configuration of three types of bias lines can be seen in Fig. 2. The bias lines were first analytically designed using closed form equations[26, 41], and then, simulated using a full-wave electromagnetic solver, HFSS[25]. During the simulations, all bias lines are terminated with open-circuited terminations. Here, this type of termination is used on purpose instead of a short-circuited termination in order not to exaggerate the loading effect.

The first type of bias line is the direct connection to the antenna, which actually forms a transmission line and is known in the literature as coplanar stripline (CPS) (Fig. 2(a))[26]. The HFSS simulation results of a CPS bias line are presented in Fig. 3(a), and it shows a typical transmission line behavior with a high magnitude of transmission coefficient, $|S_{21}|$, forming a direct path between the probe pads and antenna. In addition to that, the bias lines behave as a part of the antenna and contribute to the radiation because of the strong terahertz current leakage on the bias lines. The photonic band gap (PBG) bias lines are used as a better alternative to the CPS bias lines, which are shown in Fig. 2(b). The

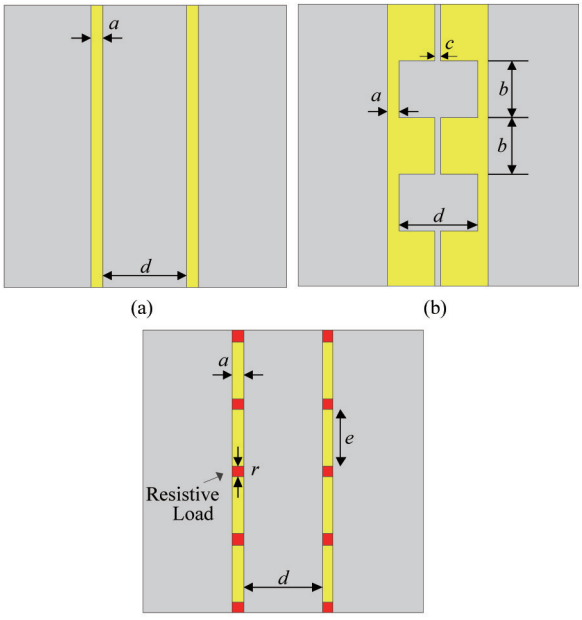

Figure 2　The DC bias lines types: (a) CPS, (b) PBG, (c) RLL

PBG bias lines are designed as a low-pass filter[27] to avoid the direct path between the probe pads and antenna. An example performance of a PBG bias line is given in Fig. 3(b). Here, the PBG bias line is designed to have a corner frequency that is fairly lower than 400 GHz, so that it provides a good isolation around 400 GHz. Although the performance is better compared with the CPS bias lines above the cut-off frequency, the PBG bias lines occupy a large metal area, which drastically loads the antenna. Moreover, the PBG bias lines are still not sufficient for wide band applications, since the cut-off frequency of the PBG bias line must be selected at a low frequency, causing the PBG bias line dimensions to grow extensively. Using CPS and PBG bias lines also bring additional losses and decrease antenna efficiency as the leakage current towards the bias lines do not contribute to the radiation and lost as resistive loss on the bias lines.

Figure 2(c) presents the proposed resistively loaded line (RLL) type bias line. The proposed idea was previously introduced for MEMS reconfigurable antennas working in the microwave and millimeter-wave frequencies[28-29]. The RLL is formed by periodically placing thin-film, lumped resistors on the CPS bias line, forming a distributed structure. In this case, the CPS bias line length is divided into much smaller lengths that become much shorter than the wavelength in the band of interest so that they do not load the antenna. In addition to that, the RLL prevents the current leakage on the bias lines and guarantees the isolation between the probe pads and antenna in a wide frequency band, which is shown in Fig. 3(c). Therefore, the distortion on the antenna radiation characteristics is expected to be minimized when the RLL bias lines are used.

For all of the three types of bias lines, whose performances are presented in Fig. 3, the design target is to minimize the coupling of the generated terahertz signal to the other end of the bias lines as much as possible, and the targeted antenna has a center frequency of 400 GHz. So, all three types of bias lines were optimized to get the minimum leakage currents, and the performances should

be compared considering how much and in what bandwidth the leakage current is suppressed.

The lumped resistances of the RLL lines were implemented as thin-film SiCr or TaN resistors. The conductivity of these layers can be tuned so that the lumped resistance can be easily adjusted in 100 Ω-100 kΩ range. During this study, the lumped resistances are selected starting from 1 kΩ, as resistance values less than 1 kΩ did not provide good isolation. Although resistance values up to 30 kΩ are applied for different types of antennas, a resistance level of a few kΩ is sufficient to provide good isolation and recover the original antenna performance (without any bias lines) for most of the cases. The loss introduced by the RLL in Fig. 2(c) is less than 10% up to 750 GHz for a resistance value of 5 kΩ, and it can be reduced to less than 2% by decreasing the periodicity, *e*. The price paid here will be the increase in the total DC resistance of the RLL.

The only drawback of using RLL bias lines for the photomixer antennas is that the applied DC voltage needed for the operation of the photomixer antenna is increased. This is because the RLL adds series resistances between the probe pads and antenna. Typically, the total resistance is in the order of 5 kΩ-to-30 kΩ. Considering that DC photoconductance of the photomixers is in the order of $(10\ \text{k}\Omega)^{-1}$ [15], the bias voltage should be roughly increased by 1/2 to 3 times of its original value. The reader should remember here that, the effective DC voltage seen by antenna remains unchanged, and hence, the operation of the antenna is not affected by the addition of the RLL bias lines. There may also be a slight increase in the noise figure of the photomixer due to the resistors of the RLL, which can be minimized by the proper design of the RLL and antenna.

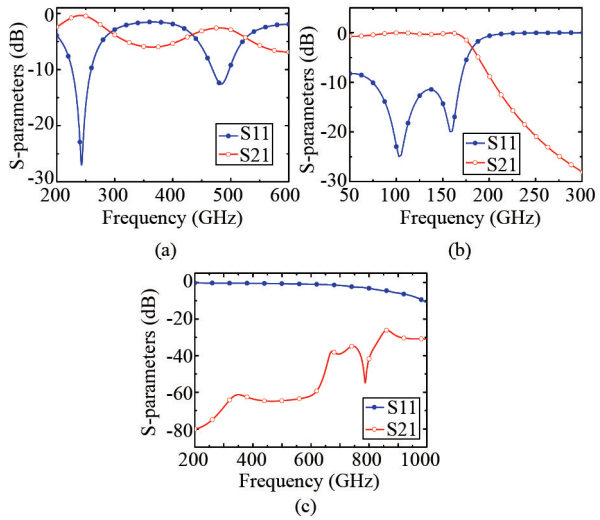

Figure 3 Two-port simulation results for the different types of bias lines (a) CPS, (b) PBG, and (c) RLL

2 Application to photomixer antennas

Different types of antennas were investigated in order to test the improvement that is offered by the RLL bias lines. These antennas include the most commonly used photomixer antennas types such as dipole[30-31], folded dipole[32], log periodic[33-34], and spiral antennas[35-36]. The antennas were first theoretically designed[24], and then, verified using HFSS. The excitation of the antennas were obtained using current sources to draw an analogy for the optical excitation, and Perfectly Matched Layer (PML) boundary conditions were used in order to exclude the edge effects that are caused by the edges of the semiconductor substrate. Other types of boundary conditions were also tested, but it was observed that the original antenna performance, which is the critical checkpoint for this study, is suppressed by the edge effects in this case. The metal parts of the antennas were implemented as perfect electric conductors (PECs) without any thickness in order to see the effects of the lumped resistances of RLL bias lines on the antenna efficiency more clearly. After the antennas were designed without the presence of any bias lines, each of the aforementioned bias lines was connected to the designed antenna to investigate their effects on the performance of the antenna.

2.1 Dipole antenna

A λ-long dipole antenna operating at a center frequency of 400 GHz is designed as the first test structure, which is shown in Fig. 4(a). The design parameters of the dipole antenna and bias lines are given in Table 1. The simulation results for the antenna with different types of bias lines are shown in Fig. 4(b) and Fig. 4(c). It is seen from the simulation results that the CPS and PBG bias lines change the antenna impedance and operation frequency, whereas RLL bias line keeps the operation frequency almost the same as the original antenna. It was also observed that the RLL bias line hardly affects the radiation pattern while the former two types distort the radiation pattern. This behavior can be more clearly understood once the current distributions are examined for all cases, which is presented in Fig. 5. Once the CPS bias line is used, a considerable amount of current leakage is noted on the bias lines; moreover, a standing wave pattern is clearly observed as expected, proving the trans-

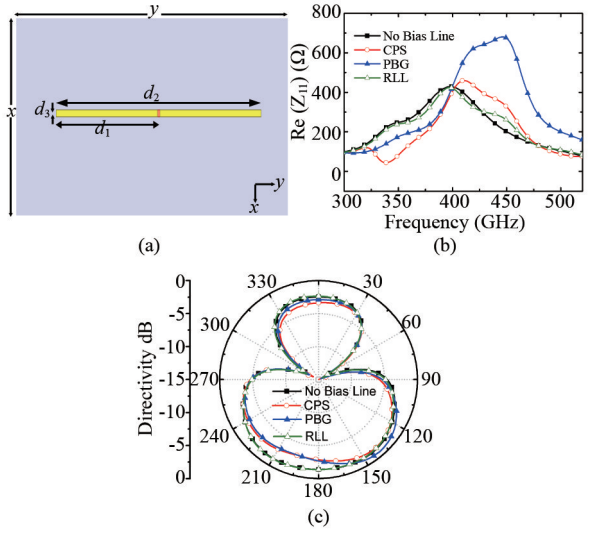

Figure 4 (a) The layout of the designed dipole antenna (b)-(c) The simulation results for the dipole antenna: (b) real part of the input impedance, (c) directivity (at 398.5 GHz)

mission line behavior (Fig. 5(a)). Although the amount of current leakage on the bias line decreases when the PBG bias line is used (Fig. 5(b)), it still has a notable effect on antenna radiation pattern (Fig. 4(c)). On the other hand, the intensity of current leakage on the bias lines are reduced extensively when the RLL bias line is selected, and therefore, having the closest input impedance and radiation pattern performance compared with that of the no bias line scenario is explained.

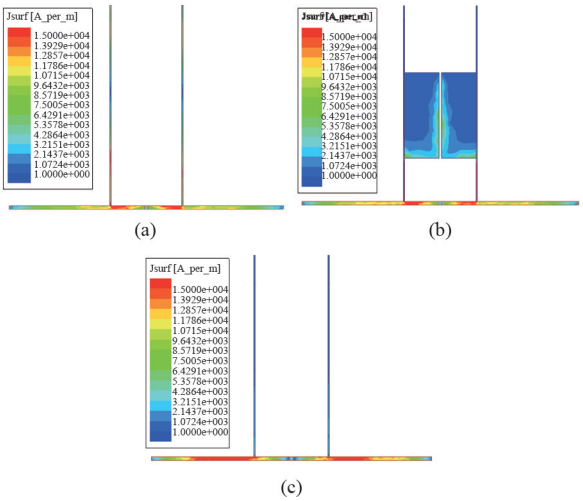

Figure 5　The current distributions for the dipole antenna at 398.5 GHz with different types of bias lines: (a) CPS, (b) PBG, (c) RLL

It should also be underlined here that, although not covered within the frame of this study, a significant amount of efficiency drop is expected due to the finite conductivity of the metals used in practical photomixer antennas, which is caused by the leakage currents on the thin, narrow, and long bias lines. So, the prevention of the leakage current is critical and expected to improve the antenna efficiency drastically. The effects of the RLL bias lines on the antenna efficiency are discussed in the following sections.

Table 1　The design parameters of the dipole antenna

Antenna and substrate parameters				Bias line parameters			
Parameter	Value (μm)	Parameter	Value (μm)	Parameter	Value (μm)	Parameter	Value (μm)
d_1	114.5	x	600	a	1	d	60
d_2	232	y	400	b	70	e	70
d_3	3			c	2	r	1

Table 2　The design parameters of the folded dipole antenna

Antenna and substrate parameters				Bias line parameters			
Parameter	Value (μm)	Parameter	Value (μm)	Parameter	Value (μm)	Parameter	Value (μm)
f_1	28.5	x	600	a	1	d	20
f_2	58	y	400	b	70	e	70
f_3	15			c	1	r	1

2.2　Folded dipole antenna

Folded dipole antennas were also employed as photomixer antennas due to their nature of having high radiation resistance. For this purpose, a folded dipole antenna was designed at 400 GHz (Fig. 6(a)), where the design parameters and results can be found in Table 2 and Figure 6, respectively. It is seen that the CPS and PBG bias lines reduce the radiation resistance considerably, shift the operating frequency, and narrow the bandwidth of the antenna (Fig. 6(b)). On the other hand, the RLL bias line causes a much lower radiation resistance drop and operating frequency shift, and the bandwidth of the antenna stays almost the same. Additionally, the CPS and PBG bias lines distract the radiation pattern of the antenna (Fig. 6(c)) due to the considerable amount of the current leakage on the bias lines, while the RLL bias line shows quite similar behavior with the radiation pattern of original antenna, since the leakage current is blocked by lumped resistances.

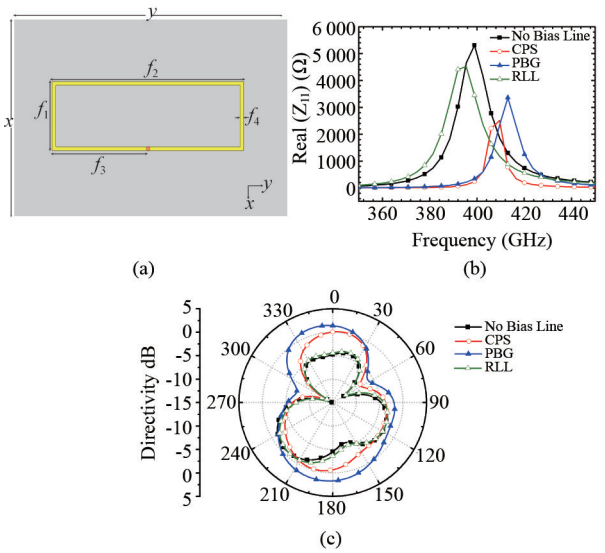

Figure 6　(a) The layout of the designed dipole antenna (b)-(c) The simulation results for the folded dipole antenna: (b) real part of the input impedance, (c) directivity (at 399 GHz)

2.3　Log periodic antenna

In order to investigate the RLL bias line performance in broadband antennas, a log periodic antenna was designed (Fig. 7(a)) to operate in 400-700 GHz frequency band with the parameters given in Table 3. Considering the simulations results in Fig. 7, one can observe that using the CPS and PBG bias lines distort the antenna characteristics. The resonance frequencies are shifted and the radiation resistances are reduced significantly, especially for the third resonance around 670 GHz. The radiation patterns are also affected, which can be seen in Fig. 7(c) as an example. A strong leakage current can be observed for the CPS and PBG bias line cases and almost no leakage current is observed for the RLL bias line case.

2.4　Spiral antenna

A high radiation resistance spiral antenna was designed as the final test structure with a center frequency of 470 GHz, which is shown in Fig. 8(a). The antenna is simulated using the same setup defined previously, and the design parameters are given in Table 4. The simulation results Fig. 8(b) show that the antenna has an input impedance of 2 337 Ω at 468 GHz when no bias lines are connected. It is clearly observed from the simulation re-

sults that the input impedance, hence, the radiation resistance, is severely reduced in case of using the CPS and PBG bias lines. The input impedance for the CPS and PBG bias line cases are 279 Ω and 174 Ω (both simulated at 492 GHz), respectively. Alternatively, the RLL bias line results in an input impedance of 1 776 Ω, which is 6 times and 10 times better than that of the CPS and PBG bias lines, respectively; moreover, it keeps the operating frequency at almost same value compared with the original antenna with no bias lines. It is seen from the simulations results that the CPS and PBG bias lines have a significant intensity of current leakage into the bias lines, and as a result, the radiation patterns of the antennas with these bias lines have considerable changes (Fig. 8(c)). On the other hand, the current leakage into bias line is minimized when the RLL bias line is used, and the radiation pattern remains almost the same compared with the original antenna with no bias lines.

Table 3 The design parameters of the log periodic antenna

Antenna and substrate parameters				Bias line parameters			
Parameter	Value (μm)	Parameter	Value (μm)	Parameter	Value (μm)	Parameter	Value (μm)
R	47	*δ*	30	*a*	2	*d*	62
x	600	*β*	60	*b*	42.5	*e*	42.5
y	400			c	1.5	r	2

Table 4 The design parameters of the spiral antenna

Antenna and substrate parameters				Bias line parameters			
Parameter	Value (μm)	Parameter	Value (μm)	Parameter	Value (μm)	Parameter	Value (μm)
S	44	*x*	500	*a*	2	*d*	165
Offset ang.	90	*y*	500	*b*	62	*e*	60
				c	1	*r*	2

2.5 The effects on radiation efficiency

It is expected that the lumped resistances used in the RLLs affect the radiation efficiency of the antenna. As mentioned previously, the antenna metals were modeled as PECs in order to see the effects of the RLLs clearly on the antenna efficiency. It is observed from the simulation results of the four antennas that the radiation efficiency is reduced at most 2% when RLL bias lines are employed, and the radiation efficiency can be increased further by increasing the value of the lumped resistances. The lumped resistance values used range from 5 kΩ-to-30 kΩ, and increasing the value of the resistance does not affect the voltage seen by the antenna, which means that the operation of the antenna remains unaffected. It should also be underlined once more here that the current distributions on all four types of antennas show similar behavior where a significant amount of leakage current is present for CPS and PBG bias lines and the usage of the lumped resistances in RLL bias lines effectively blocks the leakage current. This is an important result because the leakage currents on the thin, narrow, and long bias lines is expected to cause a considerable amount of resistive power loss, which will decrease the antenna efficiency notably. So, the authors believe that using RLLs should improve the overall antenna efficiency, and hence, the antenna performance considerably.

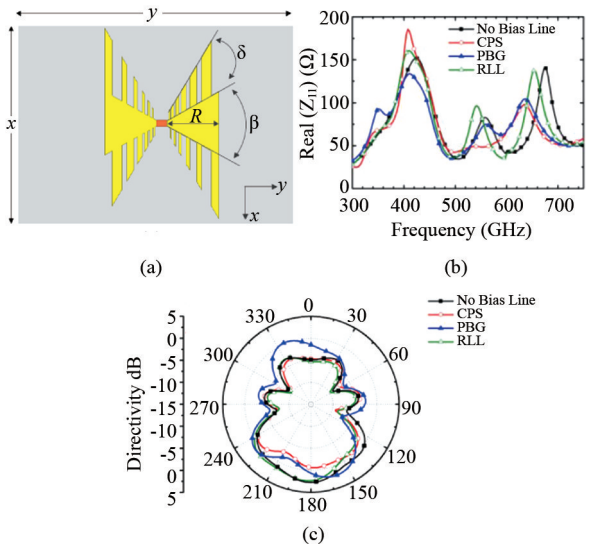

Figure 7 (a) The layout of the designed log periodic antenna (b)-(c) The simulation results for the folded dipole antenna: (b) real part of the input impedance, (c) directivity (at 558 GHz)

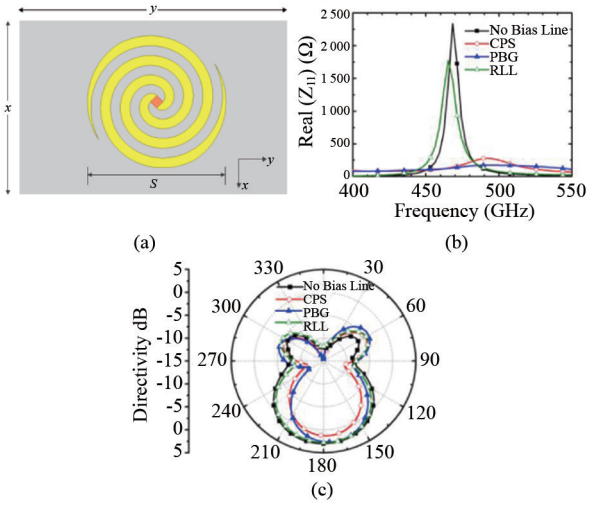

Figure 8 (a) The layout of the designed spiral antenna (b)-(c) The simulation results for the folded dipole antenna: (b) real part of the input impedance, (c) directivity (at 468 GHz)

3 Conclusion

In this study, the effects of the DC bias lines on the performance of the photomixer antennas were investigated, and the RLL bias line is proposed as a new solution for decreasing the effects of the DC bias lines and improving the antenna performance. Four types of commonly used antenna structures were examined. It is observed that using the RLL bias line improves the radiation resistance and radiation pattern characteristics compared with the CPS and PBG bias line cases; moreover, the antenna performances become very close to the original case where no bias lines are used. It is also observed that the antenna efficiency remains almost unchanged with the applica-

tion of the RLL bias lines; in addition to that, the overall antenna efficiency is expected to improve notably due to the diminishing of the leakage currents on the bias lines.

The application of the RLLs can also be extended to different types of antennas such as plasmonic or metamaterial type terahertz antennas[37-38], and it can be possible to make these types of antennas reconfigurable. Furthermore, with the development of novel, electrically tunable resistivity materials, it can also be possible to make PCAs or photomixer antennas reconfigurable by changing the RLL resistance values, and therefore, changing the RLL impedance seen by the antenna.

Acknowledgments

This work was supported by TUBITAK under grant 114E089 and Yildirim Beyazit University under grant [BAP-585].

References

[1] Smith P R, Auston D H, Nuss M C. Subpicosecond photoconducting dipole antennas [J]. *IEEE J. Quantum Electron.*, 1988, **24**(2): 255.

[2] Exter M V, Grischkowsky D. Characterization of an optoelectronic terahertz beam system [J]. *IEEE Trans. Microw. Theory Tech.*, 1990, **38**(11): 1684-8.

[3] Hu B B, Nuss M C. Imaging with terahertz waves [J]. *Opt. Lett.*, 1995, **20**(16): 1716-3.

[4] Mittleman D M, Jacobsen R H, Nuss M C. T-ray imaging [J]. *IEEE J. Sel. Topics Quantum Electron.*, 1996, **2**(3): 679-14.

[5] Markelz A, Whitmire S, Hillebrecht J, Birge R. THz time domain spectroscopy of biomolecular conformational modes [J]. *Phys. Med. Biol.*, 2002, **47**(21): 3739-67.

[6] Zeitler J A, Taday P F, Newnham D A, Pepper M, Gordon KC, Rades T. Terahertz pulsed spectroscopy and imaging in the pharmaceutical setting - a review [J]. *J. Pharm. Pharmacol.*, 2007, **59**(2): 209-25.

[7] Rowe D G. Terahertz takes to the stage [J]. *Nature Photon.*, 2007, **1**: 75-3.

[8] Tonouchi M. Cutting-edge terahertz technology [J]. *Nature Photon.*, 2007, **1**: 97-9.

[9] Mukherjee P, Gupta B. Terahertz (THz) frequency sources and antennas - A brief review [J]. *Int. J. Infrared Milli.*, 2008, **29** (12): 1091-12.

[10] Siegel P H. Terahertz technology [J]. *IEEE Trans. Microw. Theory Tech.*, 2002, **50**(3): 910-19.

[11] Ferguson B, Zhang X C. Materials for terahertz science and technology [J]. *Nature Materials.*, 2002, **1**: 26-8.

[12] Berry C W, Wang N, Hashemi M R, Unlu M, Jarrahi M. Significant performance enhancement in photoconductive terahertz optoelectronics by incorporating plasmonic contact electrodes [J]. *Nature Commun.*, 2013, **4**: 1622-11.

[13] Nguyen T K, Kim S, Rotermund F, Park I. Design of a wideband continuous-wave photomixer antenna for terahertz wireless communication systems [J]. *J. Electromagn. Waves Appl.*, 2014, **28**(8): 976-13.

[14] Diao J M, Du L, Ouyang J, Yang P, Nie Z P. Enhanced center frequency of terahertz pulse emission from photoconductive antenna [J]. *J. Electromagn. Waves Appl.*, 2011, **25**(16): 2236-8.

[15] Brown E, Smith F, McIntosh K. Coherent millimeter-wave generation by heterodyne conversion in low-temperature-grown GaAs photoconductors [J]. *J. Appl. Phys.*, 1993, **73**(3): 1480-5.

[16] Matsuura S, Tani M, Sakai K. Generation of coherent terahertz radiation by photomixing in dipole photoconductive antennas [J]. *Appl. Phys. Lett.*, 1997, **70**(5): 559-3.

[17] Peytavit E, Mouret G, Lampin J, Arscott S, Masselin P, Desplanque L, Vanb? esien O, Bocquet R, Mollot F, Lippens D. Terahertz electromagnetic generation via optical frequency difference [J]. *P. IEEE-Optoelectron.*, 2002, **149**(3): 82-6.

[18] Nguyen T K, Ho T A, Park I, Han H. Full-wavelength dipole antenna on a GaAs membrane covered by a frequency selective surface for a terahertz photomixer [J]. Prog. *Electromagn. Res.*, 2012, **131**: 441-15.

[19] Mandviwala T, Lail B, Boreman G. Infrared-frequency coplanar striplines: design, fabrication, and measurements [J]. *Microw. Opt. Technol. Lett.*, 2005, **47**(1): 17-3.

[20] Nguyen T K, Park I. Effects of antenna design parameters on the characteristics of a terahertz coplanar stripline dipole antenna [J]. *Prog. Electromagn. Res. M.*, 2013, **28**: 129-15.

[21] Han K, Nguyen T K, Park I, Han H. Terahertz Yagi-Uda antenna for high input resistance [J]. *Int. J. Infrared Milli.*, 2010, **31**(4): 441-14.

[22] Duffy S M, Verghese S, McIntosh K A, Jackson A, Gossard AC, Matsuura S. Accurate modeling of dual dipole and slot elements used with photomixers for coherent terahertz output power [J]. *IEEE Trans. Microw. Theory Tech.*, 2001, **49**(6): 1032-7.

[23] Zhu N, Ziolkowski R W. Photoconductive THz antenna designs with high radiation efficiency, high directivity, and high aperture efficiency [J]. *IEEE Trans. THz Sci. Technol.*, 2013, **3**(6): 721-10.

[24] Balanis C A. *Antenna Theory: Analysis and Design* [M]. New Jersey, USA: Wiley, 1997.

[25] High frequency structural simulator. Pittsburgh (PA): Ansoft Corp; 2010.

[26] Collin R E. *Foundation for Microwave Engineering* [M]. New York, USA: IEEE Press, 2011.

[27] Akalin T, Laso M A G, Lopetegi T, Vanbesien O, Sorolla M, Lippens D. PBG-type microstrip filters with one and two-sided patterns [J]. *Microw. Opt. Technol. Lett.*, 2001, **30**(1): 69-4.

[28] Zohur A, Mopidevi H, Rodrigo D, Unlu M, Jofre L, Cetiner B A. RF MEMS reconfigurable two-band antenna [J]. *IEEE Antennas Wireless Propag. Lett.*, 2013, **12**: 72-4.

[29] Unlu M, Damgaci Y, Mopidevi H S, Kaynar O, Cetiner B A. Reconfigurable, tri-band RF MEMS PIFA antenna [J]. *P. IEEE Int. AP-S Symp.*, 2011.

[30] Miyamaru F, Saito Y, Yamamoto K, Furuya T, Nishizawa S, Tani M. Dependence of emission of terahertz radiation on geometrical parameters of dipole photoconductive antennas [J]. *Appl. Phys. Lett.*, ? 2010, **96**(21): 211104-3.

[31] Dragoman D, Dragoman M. Terahertz fields and applications [J]. *Prog. Quant. Electron.*, 2004, **28**(1): 1-67.

[32] Ryu H C, Kim S I, Kwak M H, Kang K Y, Park S O. A folded dipole antenna having extremely high input impedance for continuous-wave terahertz power enhancement. *P. IRMMW-THz.*, 2008.

[33] Gitin M M, Wise F W, Arjavalingam G, Pastol Y, Compton

R C. Broad-band characterization of millimeter-wave log-periodic antennas by photoconductive sampling [J]. *IEEE Trans. Antennas Propag.*, 1994, **42**(3): 335-5.

[34] Mendis R, Sydlo C, Sigmund J, Feiginov M, Meissner P, Hartnagel H L. Tunable CW-THz system with a log-periodic photoconductive emitter [J]. *Solid-State Electron.*, 2004, **48**(10): 2041-5.

[35] Sizov F, Rogalski A. THz detectors [J]. *Prog. Quant. Electron.*, 2010, 34(5): 278-70.

[36] Gregory I S, Baker C, Tribe W R, Bradley I V, Evans M J, Linfield E H, Davies A G, Missous M. Optimization of photomixers and antennas for continuous-wave terahertz emission [J]. *IEEE J. Quant. Electron.*, 2005, **41**(5): 717-12.

[37] Yang Y, Singh R, Zhang W. Anomalous terahertz transmission in bow-tie plasmonic antenna apertures [J]. *Opt. Lett.*, 2011, **36**(15): 2901-3.

[38] Gu J, Han J, Lu X, Singh R, Tian Z, Xing Q, Zhang W. A close-ring pair terahertz metamaterial resonating at normal incidence [J]. *Opt. Express.*, 2009, **17**(22): 20307-6.

[39] Focardi P, McGrath W R, Neto A. Design guidelines for terahertz mixers and detectors [J]. *IEEE Trans. Microw. Theory Tech.*, 2005, **53**(5): 1653-9.

[40] Nguyen T K, Park I. Impact of varying the DC bias stripline connection angle on terahertz coplanar stripline dipole antenna characteristics [J]. *J. Electromagn. Waves Appl.*, 2013, **27**(14): 1725-10.

[41] Guo B, Wen J H, Zhang H C, Zhong W B, Lin W Z. Terahertz dispersion and attenuation characteristics of optically excited coplanar striplines on LT-GaAs [J]. *J. Infrared Millim. W.*, 2000, **19**(2): 98-102.